J Appl Electrochem (2014) 44:555–562
DOI 10.1007/s10800-014-0675-1

RESEARCH ARTICLE

Synthesis and characterization of Pt-doped $LiFePO_4$/C composites using the sol–gel method as the cathode material in lithium-ion batteries

M. Talebi-Esfandarani · O. Savadogo

Received: 16 November 2013 / Accepted: 3 February 2014 / Published online: 16 February 2014

Abstract $LiFePO_4$/C and $LiFe_{0.96}Pt_{0.04}PO_4$/C nanocomposite cathode materials were synthesized using the sol–gel method in a nitrogen atmosphere. The samples were characterized by X-ray diffraction (XRD), X-ray photoelectron spectroscopy (XPS), and scanning electron microscopy (SEM). Their electrochemical properties were investigated using galvanostatic charge/discharge tests, cyclic voltammetry (CV), and electrochemical impedance spectroscopy (EIS). The XRD results indicate that substituting iron with platinum does not destroy the structure of $LiFePO_4$, but expands the lattice parameters and enlarges the cell volume. The electrochemical results show that platinum doping improves the electrochemical performance of $LiFePO_4$/C particles owing to the expansion of the lattice structure, which provides more space for Li ion diffusion. The, larger lattice structure parameters of the $LiFe_{0.96}Pt_{0.04}PO_4$/C material result in a high discharge capacity of 166, 156, 142 and 140 mAh g^{-1} at rates of 0.2, 1, 5, and 10 C, respectively, as compared to 164, 150, 120, and 105 mAh g^{-1} for undoped $LiFePO_4$/C.

Keywords $LiFePO_4$/C · Sol–gel method · Platinum doping

1 Introduction

$LiFePO_4$ has been chosen as a promising candidate for cathode materials in lithium-ion battery applications because of features like low cost, abundance in nature, excellent thermal stability, non-toxicity, and high cyclability [1, 2]. However, pristine $LiFePO_4$ has its drawbacks as well: low intrinsic electrical conductivity and poor Li ion diffusion, which limit its application in large devices [3, 4]. Various strategies, including carbon coating, minimizing the particle size, and element doping have been proposed to remedy these drawbacks [5–14].

Element doping has been confirmed to improve the intrinsic electrical conductivity of $LiFePO_4$ particles [13–15]. Moreover, a doped element causes lattice parameter expansion and enlargement of the cell volume, which induces lengthening and weakening of the Li–O bond with a lower energy barrier, and provide more space for Li ion diffusion. This facilitates Li ion movement in the $LiFePO_4$ structure, increases ionic conductivity, and improves the electrochemical performance of the $LiFePO_4$ material [16–18]. Furthermore, the doped element in the lattice structure can act as a pillar to prevent the collapse of the crystal structure during the charge/discharge process, which is indicative of good electrochemical performance [19, 20].

It is well accepted that there are mainly two different doping modes of $LiFePO_4$: inserting the doping element in the M_1 (lithium site) sites or inserting the doping element in the M_2 (iron site) sites. Doping at the M_1 sites might help to compensate the lithium vacancy which may improve the electrochemical performance of the doped $LiFePO_4$. However, the doping element at this site can become immobile. The presence of this unmoving doping element at the Li site may probably block the channel for the diffusion of Li^+ ions [21]. Therefore, doping at M_2 site where the doping element will not block the Li^+ ions diffusion through the Li movement channel is very interesting. This last case could be an ideal and promising

M. Talebi-Esfandarani · O. Savadogo (✉)
Laboratory of New Materials for Electrochemistry and Energy, Polytechnique Montréal, C.P. 6079, Succ. Centre Ville, Montréal, QC H3C 3A7, Canada
e-mail: osavadogo@polymtl.ca

way to improve the electrochemical performance of $LiFePO_4$ due to the enhancement of the Li^+ ions diffusion. This is why in this work, metal doping is carried out on the M_2 site.

Consequently, doping at the M_2 site might be a better choice for enhancing Li ion diffusion. For some parameters, including physical–chemical properties, the amount of the doping element and the ionic radius must be taken into consideration.

However, Nazar et al. report that the improved electrical conductivity is caused by the formation of a conductive film of Fe_2P on the doped samples, and not the doping element [22]. Also, theoretical studies indicate that element doping on $LiFePO_4$ is not useful [23], since $LiFePO_4$ has a one-dimensional Li ion diffusion pathway [24, 25] and also because the large amount of an unmoving doped element at the M_1 site may block the channel for Li ion diffusion and decrease electrochemical performance [26, 27]. However, various doping elements, such as Ti [9], Cu [10], La [18], Ru [19], Zn [20], Co [28], Na [29], V [30], Mg [31], etc., have been proposed to improve the electrochemical performance of $LiFePO_4$.

Up to now, the effect of platinum on the structure and electrochemical properties of $LiFePO_4$ has not been reported. In this article, Pt-doped $LiFePO_4$ material is synthesized using the sol–gel method, and the effect of Pt doping on the structure and electrochemical properties of $LiFePO_4$/C is investigated.

2 Experimental

2.1 Synthesis of materials

The $LiFePO_4$ and $LiFe_{0.96}Pt_{0.04}PO_4$ samples were synthesized using the sol–gel method. The precursor materials were $Li(CH_3COO)$ (lithium acetate, Alfa Aesar), $Fe(NO_3)_3{\cdot}9H_2O$ (iron nitrate, Sigma Aldrich), $H_2PtCl_6{\cdot}6H_2O$ (hexachloroplatine, Alfa Aesar), H_3PO_4 (phosphoric acid, Anachemia), and $C_2H_4O_3$ (glycolic acid, Sigma Aldrich). We first mixed the platinum and iron precursors in the solvent to dissolve them completely. This help first to insert the doping metal ion (Pt ion) in the M_2. Then, we add the lithium precursor to the above solution. For the synthesis of the $LiFePO_4$ sample, phosphoric acid was diluted in distilled water and metal precursors were added to the solution while stirring, until completely dissolved. The solution was mixed slowly with glycolic acid and the pH was adjusted to fall in the 8.5–9.5 range using ammonium hydroxide. The solution was heated at 90 °C while stirring, until a gel formed under a nitrogen atmosphere. After drying at 120 °C in a vacuum oven for 48 h, the sample was annealed at 500 °C for 10 h in a nitrogen flow to obtain $LiFePO_4$ powders. For the synthesis of the $LiFe_{0.96}Pt_{0.04}PO_4$ sample, 4 mol % of the iron nitrate was replaced by 4 mol % of hexachloroplatine. Finally, the pre-synthesized $LiFePO_4$ and $LiFe_{0.96}Pt_{0.04}PO_4$ samples were mixed with sucrose as the carbon source in a 70:30 weight ratio, followed by calcination at 700 °C for 5 h in a nitrogen atmosphere to obtain a $LiFePO_4$/C and $LiFe_{0.96}Pt_{0.04}PO_4$/C composite.

2.2 Materials characterization

The crystal structure and cell parameters of the samples were identified using an X-ray diffractometer (XRD, Philips X'pert) with Cu K_α radiation ($\lambda = 1.54056$ Å). The oxidation states of the Fe and Pt ions were analyzed by X-ray photoelectron spectroscopy (XPS, VG ESCALAB 3 MKII) with an Al K_α radiation source ($h\nu = 1486.6$ eV). The data were calibrated with respect to the C 1s peak at a fixed value of 285.0 eV. The morphology and particle size were examined by scanning electron microscopy (SEM, JSM-7600TFE). The carbon content of the samples was measured by carbon analyzer (LECO Co., CS 400).

2.3 Electrochemical characterization

The composite cathode materials for the electrochemical tests were prepared by mixing 80 % active material, 10 % carbon black (Super C65-Timcal), and 10 % poly vinylidene fluoride (PVDF) in *N*-methyl-2-pyrrolidone solvent. Then, the slurry was used to coat an aluminum foil current collector using the doctor blade technique and dried in vacuum oven overnight. The dried electrodes, with an area of 1.77 cm^2 and containing 2–4 mg of active materials, were used as the cathode material in the cells. The cells (2032) were assembled in an argon-filled glove box with lithium metal as the anode (as the counter and reference electrodes), and a Celgard 2400 separator. $LiPF_6$ (1 M) in a 1:1 volume ratio of ethylene carbonate to dimethyl carbonate (LP30 from Merck) was used as the electrolyte. The charge/discharge test and cycling stability test were performed at different current rates over a 2.5–4.2 V voltage range with the Solartron battery test analyser. Cyclic voltammetry (CV) was carried out using PAR273A in the potential ranges of 2.5–4.2 V (vs. Li/Li^+) with scan rates of 0.1 mV s^{-1}. The electrochemical impedance spectrum (EIS) measurements were taken using the Solartron 1260 in a frequency range of 0.01 Hz–1 mHz at the discharge status of the cells.

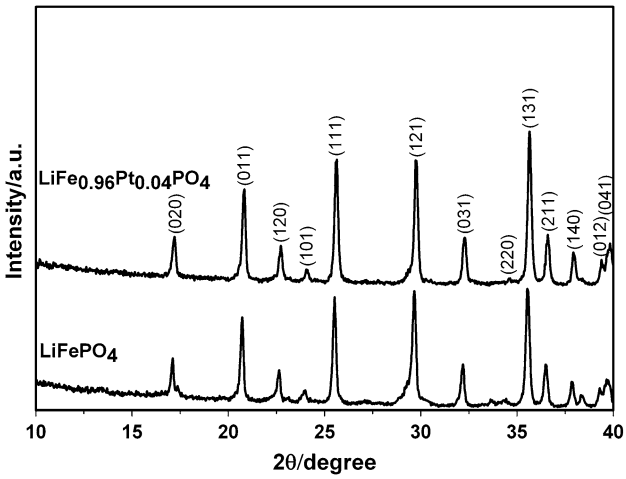

Fig. 1 XRD patterns of $LiFePO_4$ and doped $LiFe_{0.96}Pt_{0.04}PO_4$ samples

3 Results and discussion

The XRD patterns for the $LiFePO_4$ and $LiFe_{0.96}Pt_{0.04}PO_4$ samples are shown in Fig. 1. For both samples, the main diffraction peaks identify a single phase of $LiFePO_4$ olivine structure indexed by an orthorhombic space group of P_{mnb} (JCPDS 40-1499). The impurity phases, such as Li_3PO_4 and Fe_2P, were not detected for either sample. Li_3PO_4 has usually been reported as an impurity in doped $LiFePO_4$ samples, which reduces electrochemical performance [9, 14, 32]. For the $LiFe_{0.96}Pt_{0.04}PO_4$ samples, we observe an increase in the intensities of the diffraction peaks, indicating that platinum doping enhances the degree of crystallinity. Effectively, the measuring set up of all both samples (un-doped and Pt-doped samples) such as amount and thickness of the powder in the sample holder and also the experimental characterization parameters were the same. Therefore, an increase in the intensity of the diffraction peaks of $LiFe_{0.96}Pt_{0.04}PO_4$ indicates an increase in the sample crystallinity. This indicates that platinum doping enhances the degree of crystallinity of $LiFePO_4$. This is an indication that Pt doping of $LiFePO_4$ can help in the formation of a better crystal of this cathode material. Particles with well-shaped crystallinity are essential for enhancing the electrochemical performance of $LiFePO_4$ materials [2]. Considering the proper degree of crystallinity, the $LiFe_{0.96}Pt_{0.04}PO_4$ sample is expected to show enhanced electrochemical performances compared with $LiFePO_4$, which we explain in the electrochemical results section.

The lattice parameters of the samples, which were calculated from XRD patterns using Topas software, are summarized in Table 1. The results in Table 1 show that there are significant changes in the third decimal for the *a*, *b*, and *c* lattice parameters. These changes are significantly higher than the error which is in the fourth decimal. Also, the increasing of volume is more evidence because it is in the first decimal.

Table 1 The lattice parameters of both samples from XRD data

Sample	*a* (Å)	*b* (Å)	*c* (Å)	*V* (Å^3)	*V*%
$LiFePO_4$	10.3240	6.0028	4.6905	290.689	–
$LiFe_{0.96}Pt_{0.04}PO_4$	10.3264	6.0053	4.6921	290.974	+0.0010

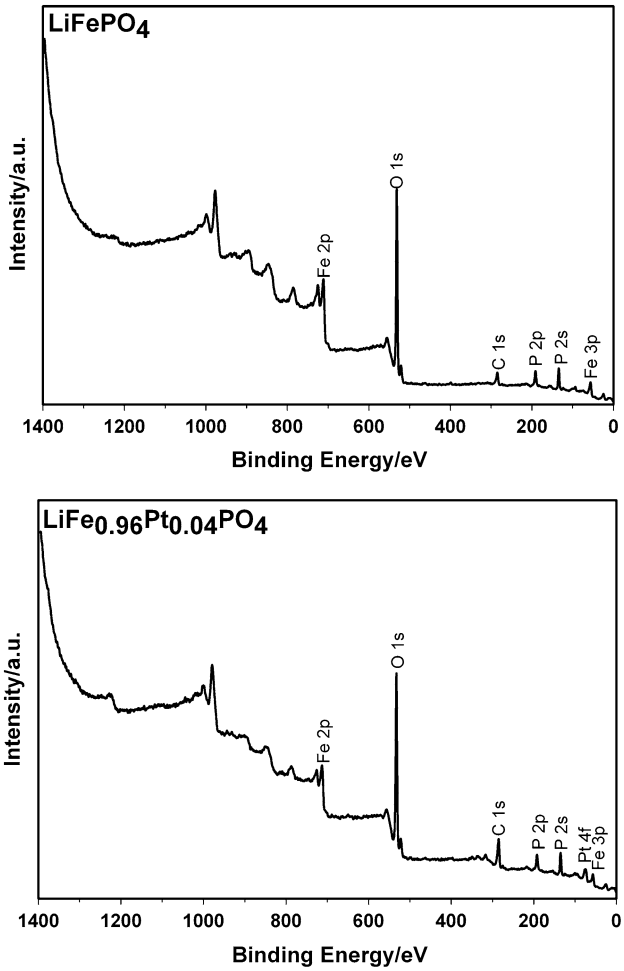

Fig. 2 XPS spectra of $LiFePO_4$ and $LiFe_{0.96}Pt_{0.04}PO_4$ samples

Owing to the Pt doping, the lattice parameters expand and the cell volume increases, indicating that the Pt has been successfully doped into the $LiFePO_4$ phase. Since the ionic radius of Pt^{2+} is larger than that of Fe^{2+}, it is reasonable that the lattice parameters increase with the doping of Pt^{2+} at the Fe^{2+} site. The expansion of the lattice parameters provides more space for Li ion diffusion and facilitates the movement of Li ions through the structure of the $LiFePO_4$ material during the intercalation and de-intercalation process. As a

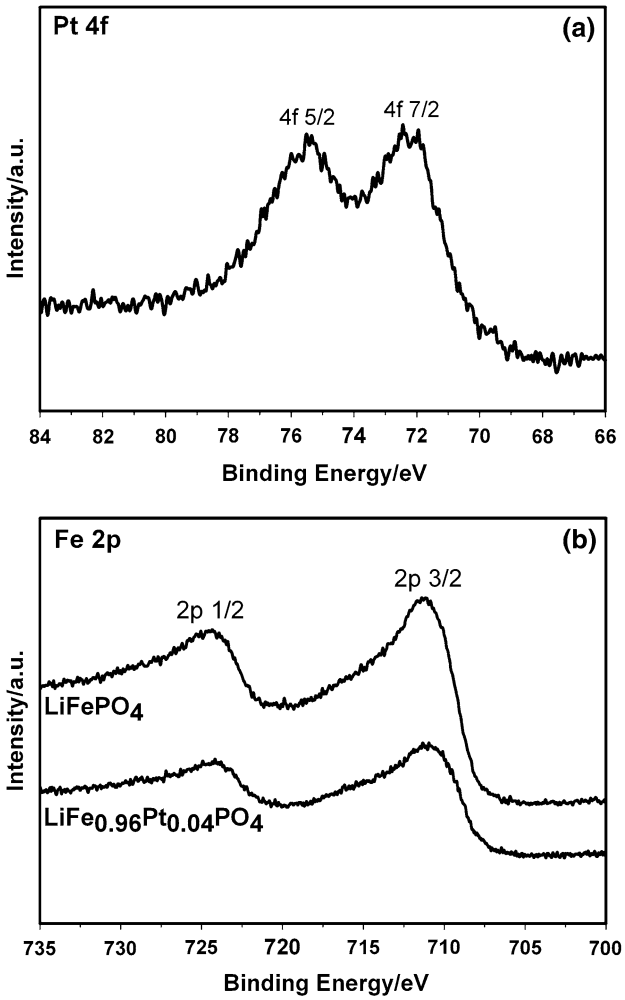

Fig. 3 **a** XPS core level of Pt 4f for $LiFe_{0.96}Pt_{0.04}PO_4$ sample. **b** XPS core levels of Fe 2p for both samples

result, the electrochemical performance of the $LiFePO_4$ material is enhanced [9, 16, 17].

XPS analysis is a powerful technique for investigating the oxidation states of Fe and Pt for the $LiFePO_4$ and $LiFe_{0.96}Pt_{0.04}PO_4$ samples. XPS spectra in a wide range of binding energies are shown for the two samples in Fig. 2. The peaks corresponding to Fe 2p, O 1s, P 2p, and C 1s were detected for both samples, and are labeled as such in Fig. 2. The binding energy for the Li 1s peak is overlapped by the Fe 3p peak (56 eV), which indicates that its binding energy and the approximation of the content of the element were prevented. It is worth noting that the Pt 4f peak was observed for the $LiFe_{0.96}Pt_{0.04}PO_4$ sample, as illustrated in Fig. 2, confirming the presence of Pt in the doped sample.

Figure 3a shows the high resolution spectrum for the Pt 4f peak for the $LiFe_{0.96}Pt_{0.04}PO_4$ sample. It contains a doublet with binding energies of 72.4 and 75.5 eV, corresponding to the Pt 4f7/2 and Pt 4f5/2 lines, respectively, and determining that the oxidation state of Pt in the doped sample is +2 [33]. This reveals that Pt^{4+} ions are partly changed into Pt^{2+} during the synthesis of the material, since the Pt precursor was in Pt^{4+} status. However, the ionic radius of Pt^{2+} (80 Å) is larger than that of Pt^{4+} (62.5 Å). Owing to the reduction of Pt^{4+} to Pt^{2+} with its larger ionic radius, it can expand the lattice parameters and enlarge the cell volume, which is compatible with the XRD result.

In order to investigate the effect of Pt doping on the binding energy and oxidation state of Fe, the high resolution spectra of the Fe 2p peak for the two samples were compared, as shown in Fig. 3b. The $LiFePO_4$ samples contain Fe 2p3/2 (710.9 eV) and Fe 2p1/2 (724 eV) peaks, indicating that the oxidation state of the Fe is +2 [28, 34]. For the doped sample, the Fe 2p3/2 (710.6 eV) and the Fe 2p1/2 (724 eV) peaks show a little shift in comparison with those of the $LiFePO_4$ sample, but Pt doping does not significantly change the valence of Fe^{2+}.

Figure 4 illustrates the SEM images of the $LiFePO_4$ and $LiFe_{0.96}Pt_{0.04}PO_4$ samples. The $LiFePO_4$ materials consist of small homogenous particles 100–500 nm in size, as shown in Fig. 4a and b. As can be seen in Fig. 4c and d, the $LiFe_{0.96}Pt_{0.04}PO_4$ particles are more homogeneous, and a more uniform particle in terms of size distribution is achieved for the doped samples. The size of the particles for the doped sample is in the 100–200 nm range. The noticeable change in terms of refining and homogenizing the size of the particles could be related to the presence of Pt during synthesis in the doped sample. This is due to the nucleation of Pt during synthesis and prevents the increase of the doped $LiFePO_4$ particles size. The use of small, homogeneous particles is a known strategy for improving the electrochemical properties of the $LiFePO_4$ material, because of the short diffusion path of the Li ions during the redox reaction [8, 11, 35, 36]. Therefore, an excellent electrochemical performance for the doped sample is expected.

Figure 5 compares the discharge curves of the $LiFePO_4$/C and $LiFe_{0.96}Pt_{0.04}PO_4$/C samples at different C-rates. The $LiFePO_4$/C sample shows a flat voltage plateau at around 3.4 V at low rates, which can be attributed to a two phase Fe^{3+}/Fe^{2+} redox process between $FePO_4$ and $LiFePO_4$ [1]. We can see that the discharge capacity of the $LiFePO_4$/C sample was strongly affected by the C-rate. The $LiFePO_4$/C sample achieves the specific capacity of 164, 150, 120, and 105 mAh g^{-1} at the rates of 0.2, 1, 5, and 10 C, respectively. The discharge capacity for the $LiFe_{0.96}Pt_{0.04}PO_4$/C sample increases to 165.95, 155.7, 142.4, and 139.5 mAh g^{-1} at rates of 0.2, 1, 5, and 10 C, respectively. Furthermore, the $LiFe_{0.98}Pt_{0.02}PO_4$/C sample shows flatter plateaus than the $LiFePO_4$/C sample at high current rates, which confirms the lower polarization for the doped sample. The content of the remaining carbon for both samples

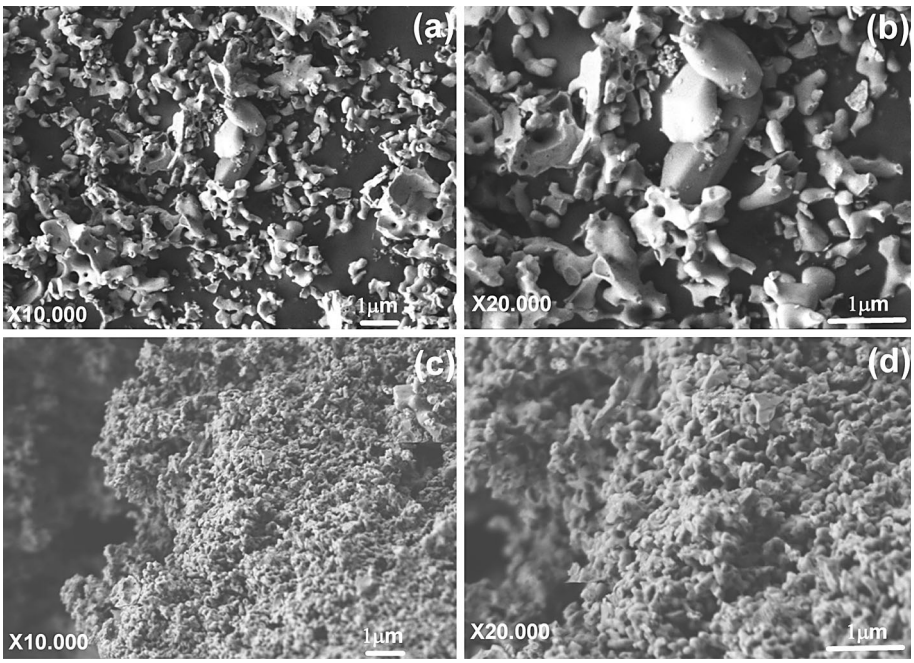

Fig. 4 Low magnification and high magnification SEM images of $LiFePO_4$ (**a**, **b**), and $LiFe_{0.96}Pt_{0.06}PO_4$ (**c**, **d**) samples

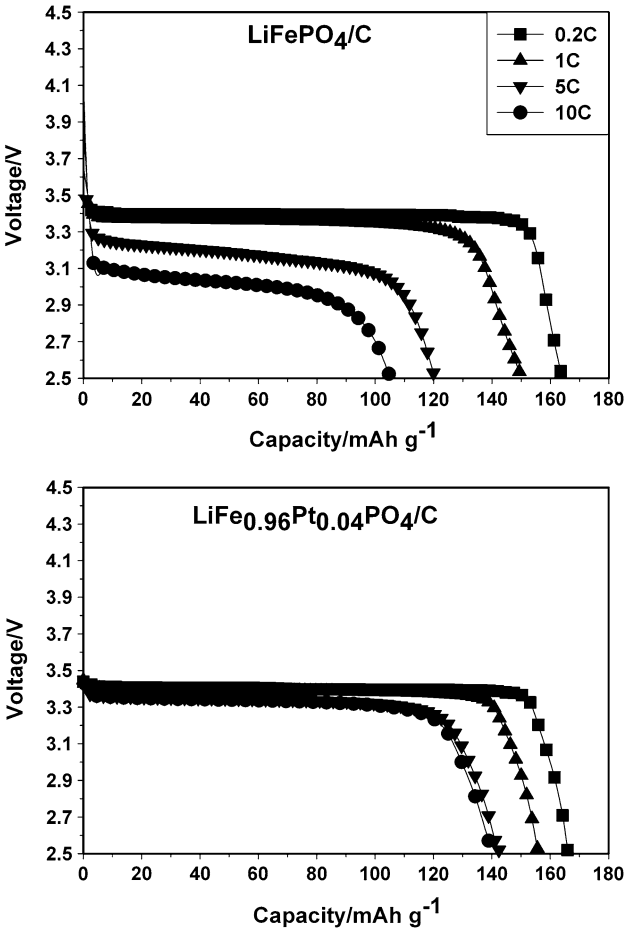

Fig. 5 The discharge curves of $LiFePO_4$/C and $LiFe_{0.96}Pt_{0.04}PO_4$/C samples at various current rates

was around 6.8 wt % which was measured by carbon analyzer (LECO). The increase in specific capacity can be related to the enhanced mobility of the Li^+ ion for the doped sample. As shown in Table 1, Pt doping causes enlargement and expansion of the lattice parameters, providing more space for the transfer of Li ions and facilitating Li ion diffusion into the $LiFePO_4$ structure, which is consistent with other reports [9, 16, 29]. Therefore, the Li^+ ion movement in the $LiFePO_4$ structure is faster, resulting in increased discharge capacities. Also, the uniform particle size distribution could offset the barrier to the sluggish charge transport of phosphate [2] and would enhance the utilization ratio of the active materials, improving electrochemical performance. This is attributed to the refinement of the particle size of $LiFePO_4$ materials and which we observed in the SEM results for the doped sample. On the other hand, these results showed clearly that the discharge capacities at high rates (5 and 10 C) of $LiFe_{0.96}Pt_{0.04}PO_4$ cathode (142 and 140 mAh g^{-1}) are significantly higher than those of $LiFePO_4$ cathode (120 and 105). This is attributed to the expansion of the lattice of $LiFe_{0.96}Pt_{0.04}PO_4$ in comparison to $LiFePO_4$ and the high diffusion of Li ion in $LiFe_{0.96}Pt_{0.04}PO_4$. We can conclude that Li^+-ion diffusion rate is the limiting parameter at high rates. This diffusion rate improves with the expansion of the material lattice parameters and the reduction of its particle sizes.

Platinum was considered as a doping element due to its high stability and activity features which can stabilize the crystal structure of $LiFePO_4$/C during charge/discharge

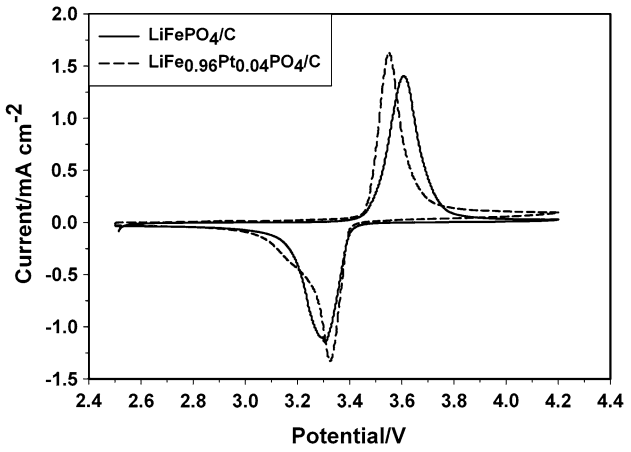

Fig. 6 The CV curves of $LiFePO_4$/C and $LiFe_{0.96}Pt_{0.04}PO_4$/C samples at the scanning rate 0.1 mV s^{-1}

process. Effectively, comparison of the best specific discharge capacities of some doped-$LiFePO_4$ materials reported in the literature to the performance of the best sample in this work ($LiFe_{0.96}Pt_{0.04}PO_4$/C prepared by sol–gel method) shows that the $LiFe_{0.96}Pt_{0.04}PO_4$/C sample delivers the specific discharge capacities of 166, 156, 142, and 140 mAh g^{-1} at current rates of 0.2, 1, 5, and 10 C, respectively, which are higher than those of the best reported data for metal-doped $LiFePO_4$/C in the literature, especially at high current rates. In particular, the specific discharge at a current rates of 10 C for $LiFe_{0.96}Pt_{0.04}PO_4$/C sample (140 mAh g^{-1}) is higher than those obtained with $LiFeP_{0.95}V_{0.05}O_4$/C [37] (100 mAh g^{-1}), $LiFe_{0.97}Sn_{0.03}PO_4$/C [38] (130 mAh g^{-1}) and F-doped $LiFePO_4$/C [39] (100 mAh g^{-1}). Accordingly, from the author's knowledge, $LiFe_{0.96}Pt_{0.04}PO_4$/C sample exhibits one of the best performances reported until now for $LiFePO_4$ materials tested in a regular cell.

Figure 6 shows the CV curves of the $LiFePO_4$/C and $LiFe_{0.96}Pt_{0.04}PO_4$/C samples at a scanning rate of 0.1 mV s^{-1} over a voltage range of 2.5–4.2 V. For both samples, the clear oxidation–reduction peaks consist of a two phase redox reaction of Fe^{2+}/Fe^{3+} in $LiFePO_4$ [10]. However, the $LiFe_{0.96}Pt_{0.04}PO_4$/C sample shows sharper and larger redox peaks with higher current, which can be attributed to an improvement in the Li^+ ion's diffusion velocity. Also, the potential separation between the oxidation–reduction peaks in the $LiFe_{0.96}Pt_{0.04}PO_4$/C sample is smaller than that in the $LiFePO_4$/C sample, suggesting lower polarization and better reversibility for the electrochemical reaction. The details of the potential values and the peak current density of the redox reactions from the CV results are listed in Table 2. The well-defined peaks and the potential separation of the smaller peaks suggest that the electrochemical properties are improved by Pt doping. For $LiFePO_4$ doped with 6 % Pt, the performance was significantly reduced even less than undoped $LiFePO_4$ cathode. $LiFe_{0.94}Pt_{0.06}PO_4$/C sample delivers the following specific discharge capacities of 135, 127, 102, and 77 mAh g^{-1} at current rates of 0.2, 1, 5, and 10 C, respectively.

For further electrochemical investigation, EIS was carried out for the two samples in the full discharge state of the cells, as shown in Fig. 7. Both samples exhibit a depressed semicircle in the high frequency region and a straight line in the low frequency region. An intercept at high frequency at the Z_{real} axis corresponds to the resistance of the electrolyte (R_e). The numerical value of the diameter of the semicircle on the Z_{real} axis in the middle frequency range is attributed to the charge transfer resistance (R_{ct}). The straight line in the low frequency range indicates the presence of Warburg impedance (Z_w), which is associated with Li ion diffusion. From the impedance curves of Fig. 7, we calculate the Li ion diffusion coefficients in the two samples which were found to be around 2×10^{-14} cm^2 s^{-1} for $LiFePO_4$ and 6×10^{-14} cm^2 s^{-1} for $LiFe_{0.96}Pt_{0.04}PO_4$. This supports the above conclusion that the discharge capacity has been increased in $LiFe_{0.96}Pt_{0.04}PO_4$ due to the faster movement of Li in this sample. The CPE represents the double layer capacitance and passivation film capacitance. An equivalent circuit is used to fit the impedance spectra, as shown in the inset in Fig. 7. The fitted impedance parameters are listed in Table 3. The charge transfer resistances (R_{ct}) of the $LiFePO_4$/C and $LiFe_{0.96}Pt_{0.04}PO_4$/C samples are 52.27 and 15.00 Ω, respectively. (The charge transfer resistance correlates to the reaction between the active materials and the electrolyte [40, 41]. The smaller resistance shows a greater possibility of Li ion movement and electron transfer on the electrode materials, so that a decrease in charge transfer resistance is beneficial during the intercalation/deintercalation process, and enhances electrochemical performance [42]. Therefore, the electrochemical properties of $LiFePO_4$/C can be improved by Pt doping, which is consistent with the CV results.

The cycling stability of the $LiFePO_4$/C and $LiFe_{0.96}Pt_{0.04}PO_4$/C samples at different C-rates is shown in Fig. 8. The cells for both samples were charged at a constant current of 1 C between 2.5 and 4.2 V, and discharged at different C-rates. For the $LiFe_{0.96}Pt_{0.04}PO_4$/C sample, we observed no obvious capacity fading over cycling at different rates, even at 10 C, which indicates good cycling performance and rate capability. Figure 8 also shows that measurements done in this range for all the current rates did not show any capacity fading for $LiFe_{0.96}Pt_{0.04}PO_4$/C; that is why we did not evaluate the cycling stability at higher cycles. However, for the $LiFePO_4$/C sample, a little capacity loss is observed at a high rate.

Table 2 The oxidation peak potential (E_{ox}), the reduction peak potential (E_{red}), potential separation (ΔE), and current density of redox reactions for the CV result in Fig. 6

Sample	E_{ox} (V)	E_{red} (V)	ΔE (V)	i_p(ox) (mA cm^{-2})	i_p(red) (mA cm^{-2})
$LiFePO_4$/C	3.60	3.30	0.30	1.40	1.15
$LiFe_{0.96}Pt_{0.04}PO_4$/C	3.55	3.32	0.22	1.63	1.33

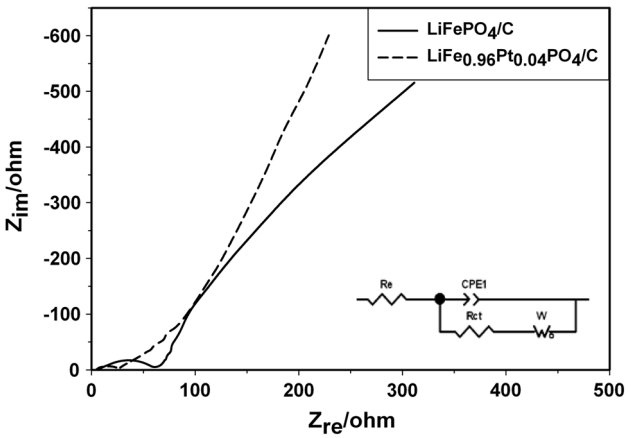

Fig. 7 EIS spectra of $LiFePO_4$/C and $LiFe_{0.96}Pt_{0.04}PO_4$/C samples. The *inset* shows an equivalent circuit of the electrode

Table 3 Impedance parameters of samples based on the equivalent circuit as inset in the Fig. 7

Sample	R_e (Ω)	R_{ct} (Ω)	CPE_1
$LiFePO_4$/C	5.67	52.27	0.6
$LiFe_{0.96}Pt_{0.04}PO_4$/C	4.68	15.00	0.7

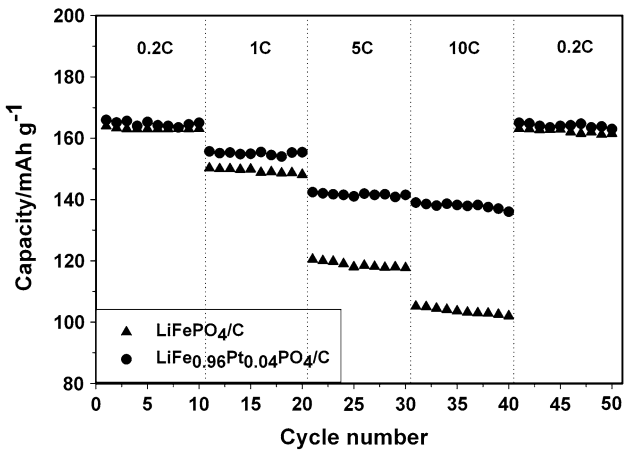

Fig. 8 Cycling performance of $LiFePO_4$/C and $LiFe_{0.96}Pt_{0.04}PO_4$/C samples at different discharge rates

Globally, the better electrochemical properties and cycling performance for the doped sample is attributed to good crystallinity, expansion of the lattice parameters, uniform particle distribution, and improved Li ion diffusion as a result of platinum doping.

4 Conclusions

The structural and electrochemical properties $LiFePO_4$/C and $LiFe_{0.96}Pt_{0.04}PO_4$/C nanocomposite cathode materials prepared using the sol–gel method were investigated. Pt doping caused lattice expansion and cell volume enlargement, providing more space for the movement of Li ions and facilitating Li ion diffusion into the $LiFePO_4$ crystal structure. In addition, a uniform particle size distribution was observed for the Pt-doped sample. The improvement in electrochemical performance can be attributed to lattice parameter expansion, uniform particle distribution, and Li ion diffusion enhancement brought about by platinum doping.

References

1. Padhi AK, Nanjundaswamy KS, Goodenough JB (1997) J Electrochem Soc 144:1188
2. Yamada A, Chung SC, Hinokuma K (2001) J Electrochem Soc 148:A224
3. Franger S, Le Cras F, Bourbon C, Rouault H (2002) Electrochem Solid-State Lett 5:A231
4. Xu Y-N, Chung S-Y, Bloking JT, Chiang Y-M, Ching WY (2004) Electrochem Solid-State Lett 7:A131
5. Zhou X, Wang F, Zhu Y, Liu Z (2011) J Mater Chem 21:3353
6. Su F-Y, You C, He Y-B, Lv W, Cui W, Jin F, Li B, Yang Q-H, Kang F (2010) J Mater Chem 20:9644
7. Doherty CM, Caruso RA, Drummond CJ (2010) Energy Environ Sci 3:813
8. Kim D-H, Kim J (2006) Electrochem Solid-State Lett 9:A439
9. Wu S-H, Chen M-S, Chien C-J, Fu Y-P (2009) J Power Sources 189:440
10. Heo JB, Lee SB, Cho SH, Kim J, Park SH, Lee YS (2009) Mater Lett 63:581
11. Yang J, Xu JJ (2006) J Electrochem Soc 153:A716
12. Kuwahara A, Suzuki S, Miyayama M (2010) J Electroceram 24:69
13. Ravet N, Chouinard Y, Magnan JF, Besner S, Gauthier M, Armand M (2001) J Power Sources 97–98:503
14. Chung S-Y, Bloking JT, Chiang Y-M (2002) Nat Mater 1:123
15. Chen J, Vacchio MJ, Wang S, Chernova N, Zavalij PY, Whittingham MS (2008) Solid State Ionics 178:1676
16. Yang M-R, Ke W-H (2008) J Electrochem Soc 155:A729
17. Liu H, Li C, Cao Q, Wu YP, Holze R (2008) J Solid State Electrochem 12:1017

18. Luo S, Tian Y, Li H, Shi K, Tang Z, Zhang Z (2010) J Rare Earths 28:439
19. Wang Y, Yang Y, Hu X, Yang Y, Shao H (2009) J Alloy Compd 481:590
20. Shenouda AY, Liu HK (2009) J Alloy Compd 477:498
21. Ellis BL, Lee KT, Nazar LF (2010) Chem Mater 22:691
22. Herle PS, Ellis B, Coombs N, Nazar LF (2004) Nat Mater 3:147
23. Islam MS, Driscoll DJ, Fisher CAJ, Slater PR (2005) Chem Mater 17:5085
24. Morgan D, Van der Ven A, Ceder G (2004) Electrochem Solid-State Lett 7:A30
25. Ouyang C, Shi S, Wang Z, Huang X, Chen L (2004) Phys Rev B 69:104303
26. Ouyang CY, Shi SQ, Wang ZX, Li H, Huang XJ, Chen LQ (2004) J Phys: Condens Matter 16:2265
27. Li D, Huang Y, Jia D, Guo Z, Bao S-J (2010) J Solid State Electrochem 14:889
28. Zhao R-R, Hung IM, Li Y-T, Chen H-Y, Lin C-P (2012) J Alloy Compd 513:282
29. Yin X, Huang K, Liu S, Wang H, Wang H (2010) J Power Sources 195:4308
30. Hong J, Wang X-L, Wang Q, Omenya F, Chernova NA, Whittingham MS, Graetz J (2012) J Phys Chem C 116:20787
31. Liu Z, Zhang X, Hong L (2009) J Appl Electrochem 39:2433
32. Axmann P, Stinner C, Wohlfahrt-Mehrens M, Mauger A, Gendron F, Julien CM (2009) Chem Mater 21:1636
33. Bancroft GM, Adams I, Coatsworth LL, Bennewitz CD, Brown JD, Westwood WD (1975) Anal Chem 47:586
34. Sun CS, Zhou Z, Xu ZG, Wang DG, Wei JP, Bian XK, Yan J (2009) J Power Sources 193:841
35. Sanchez MAE, Brito GES, Fantini MCA, Goya GF, Matos JR (2006) Solid State Ionics 177:497
36. Guo ZP, Liu H, Bewlay S, Liu HK, Dou SX (2003) J New Mater Electrochem Syst 6:259
37. Jian H, Wang CS, Chen X, Upreti S, Whittingham MS (2009) Electrochem Solid-State Letters 12:A33
38. Ma J, Li B, Du H, Xu C, Kang F (2012) J Solid State Electrochem 16:8
39. Lu F, Zhou Y, Liu J, Pan Y (2011) Electrochim Acta 56:8833
40. Liu J, Jiang R, Wang X, Huang T, Yu A (2009) J Power Sources 194:536
41. Molenda J, Ojczyk W, Marzec J (2007) J Power Sources 174:689
42. Kim J-K, Choi J-W, Chauhan GS, Ahn J-H, Hwang G-C, Choi J-B, Ahn H-J (2008) Electrochim Acta 53:8258